Taylor & Francis
Taylor & Francis Group

Combustion Science and Technology

ISSN: 0010-2202 (Print) 1563-521X (Online) Journal homepage: https://www.tandfonline.com/loi/gcst20

Effects of Mixture Distribution on Localized Forced Ignition of Stratified Mixtures: A Direct Numerical Simulation Study

Dipal Patel & Nilanjan Chakraborty

To cite this article: Dipal Patel & Nilanjan Chakraborty (2016) Effects of Mixture Distribution on Localized Forced Ignition of Stratified Mixtures: A Direct Numerical Simulation Study, Combustion Science and Technology, 188:11-12, 1904-1924, DOI: 10.1080/00102202.2016.1214415

To link to this article: https://doi.org/10.1080/00102202.2016.1214415

COMBUSTION SCIENCE AND TECHNOLOGY
2016, VOL. 188, NOS. 11–12, 1904–1924
http://dx.doi.org/10.1080/00102202.2016.1214415

Taylor & Francis
Taylor & Francis Group

Effects of Mixture Distribution on Localized Forced Ignition of Stratified Mixtures: A Direct Numerical Simulation Study

Dipal Patel and Nilanjan Chakraborty

School of Mechanical and Systems Engineering, Newcastle University, Newcastle Upon Tyne, United Kingdom

ABSTRACT

The influences of initial mixture distribution on localized forced ignition of globally stoichiometric stratified mixtures have been analyzed using three-dimensional compressible direct numerical simulations. The globally stoichiometric mixtures (i.e., $\langle\phi\rangle = 1.0$) for different root-mean-square (rms) values of equivalence ratio (i.e., $\phi' = 0.2$, 0.4, and 0.6) and the Taylor micro-scale l_ϕ of equivalence ratio ϕ variation (i.e., $l_\phi/l_f = 2.1$, 5.5, and 8.3 with l_f being the Zel'dovich flame thickness of stoichiometric mixture) have been analyzed for different initial rms values of turbulent velocity u'. The equivalence ratio variation is initialized following both Gaussian and bi-modal distributions for a given set of values of ϕ' and l_ϕ/l_f in order to analyze the effects of mixture distribution. The localized forced ignition is accounted for by considering a source term in the energy conservation equation that deposits energy for a stipulated time interval. It has been demonstrated that the initial equivalence ratio distribution has significant effects on the extent of burning of stratified mixtures following successful localized forced ignition. It has been found that an increase in $u'/S_{b(\phi=1)}$ (ϕ') has adverse effects on the burned gas mass, whereas the effects of l_ϕ/l_f on the extent of burning are non-monotonic and dependent on ϕ' for initial bi-modal mixture distribution. The initial Gaussian mixture distribution exhibits an increase in burned gas mass with decreasing l_ϕ/l_f, but these cases are more prone to flame extinction for high values of u' than the corresponding bi-modal distribution cases. Detailed physical explanations have been provided for the observed mixture distribution, ϕ', u', and l_ϕ/l_f dependences on the extent of burning following localized forced ignition of stratified mixtures.

ARTICLE HISTORY
Received 30 October 2015
Revised 22 March 2016
Accepted 22 March 2016

KEYWORDS
Direct numerical simulation (DNS); Equivalence ratio; Equivalence ratio distribution; Localized forced ignition; Stratified mixture

Introduction

Premixed combustion offers an option of controlling flame temperature and reducing pollutant (e.g., NO_x) emission, but, in practice, perfect mixing is often difficult to achieve and thus combustion in many engineering applications takes place in turbulent stratified mixtures. A number of previous analyses concentrated on flame propagation in stratified mixtures based on experimental (Anselmo-Filho et al., 2009; Balusamy et al., 2014; Grune et al., 2013; Kang and Kyritsis, 2005; Mulla and Chakravarthy, 2014; Renou et al., 2004; Samson, 2002; Sweeney et al., 2013; Zhou et al., 1998, 2013) and direct numerical simulations (DNS) (Cruz et al., 2000; Haworth et al., 2000; Hélie and Trouvé, 1998; Jiménez et al., 2002; Malkeson and Chakraborty,

CONTACT Nilanjan Chakraborty nilanjan.chakraborty@ncl.ac.uk School of Mechanical and Systems Engineering, Newcastle University, Newcastle Upon Tyne NE1 7RU, United Kingdom.

Color versions of one or more of the figures in the article can be found online at www.tandfonline.com/gcst.

2010; Patel and Chakraborty, 2014; Pera et al., 2013; Swaminathan et al., 2007) data. These studies demonstrated that the flame propagation statistics are strongly affected by the local gradient of equivalence ratio. It has been found that local variations of equivalence ratio have significant influences on the statistical behavior of surface density function (SDF) and flame curvature for small values of turbulent Reynolds number (Anselmo-Filho et al., 2009), while these effects seem to disappear when turbulence intensity increases (Sweeney et al., 2013). Recently, Pera et al. (2013) demonstrated that the mixture inhomogeneities typical of cycle-to-cycle variation in internal combustion (IC) engines can have significant influences on flame wrinkling based on mainly two-dimensional (2D) detailed chemistry DNS simulations. A similar qualitative conclusion was also drawn by Swaminathan et al. (2007) based on a preliminary analysis centered on simple chemistry 3D DNS simulations. Patel and Chakraborty (2014) have recently demonstrated, based on DNS simulations, that the root-mean-square (rms) value of equivalence ratio and the length scale of equivalence ratio fluctuations have profound influences on the extent of burning following successful forced ignition of stratified mixtures where the equivalence ratio fluctuation was initialized by a presumed bi-modal distribution.

Forced ignition of inhomogeneous mixtures arising from evaporation of droplets in an air stream has been experimentally analyzed in depth by Ballal and Lefebvre (1980) in relation to critical spark energy and optimum spark duration. Ballal and Lefebvre (1980) showed that an increase in turbulent velocity fluctuation has detrimental effects on successful ignition and early stages of combustion of inhomogeneous mixtures. Similar effects have been reported for premixed combustion based on both experimental (Ballal and Lefebvre, 1977a; Huang et al., 2007) and numerical (Chakraborty et al., 2007; Klein et al., 2008; Poinsot et al., 1995) analyses. A number of DNS-based analyses (Chakraborty et al., 2007, 2010; Chakraborty and Mastorakos, 2008) also demonstrated that an increase in turbulent velocity fluctuation for a given value of integral length scale of turbulence has a detrimental effect on the success of localized forced ignition of single-phase gaseous inhomogeneous mixtures. Recently, a similar effect has been reported by Patel and Chakraborty (2014) for localized ignition of turbulent stratified mixtures with initial bi-modal distribution of equivalence ratio. The experimental data by Ahmed and Mastorakos (2006) demonstrated that an increase in mean velocity in jets also leads to a deterioration of ignition performance, which was quantified by a reduction in ignition probability. The detrimental effects of turbulent velocity fluctuation have also been reported for localized ignition of droplet-laden mixtures (Wandel, 2013, 2014; Wandel et al., 2009).

Most existing analyses on localized forced ignition of inhomogeneous gaseous mixtures (Chakraborty et al., 2007, 2010; Chakraborty and Mastorakos, 2008) have been carried out for a mixture distribution, which is characterized by a mean variation of equivalence ratio ϕ. By contrast, localized forced ignition of stratified mixtures characterized by a constant global mean value of equivalence ratio $\langle\phi\rangle$ with non-zero rms values of equivalence ratio ϕ' has received limited attention (Patel and Chakraborty, 2014; Pera et al., 2013; Swaminathan et al., 2007) in spite of its practical importance in direct injection (DI) engines and lean premixed prevaporized (LPP) combustors. Patel and Chakraborty (2014) demonstrated that the rms value of equivalence ratio ϕ' and the length scale of equivalence ratio variation have significant influences on the early stages of combustion following localized forced ignition of stratified mixtures. Their analysis was limited to inhomogeneous mixtures with initial equivalence ratio distributions characterized by bi-modal probability density functions (pdfs). However, the effects of the nature of equivalence ratio distribution on localized forced ignition of stratified mixtures for a

given set of global mean and rms values of equivalence ratio (i.e., $\langle\phi\rangle$ and ϕ') and the associated length scale of mixture inhomogeneity are yet to be analyzed in detail. The current study aims to address the aforementioned gap in existing literature. In the current analysis, 3D compressible direct numerical simulations (DNS) have been carried out for localized forced ignition of globally stoichiometric stratified mixtures (i.e., $\langle\phi\rangle = 1.0$) for a range of different rms turbulent velocity u' for both initial Gaussian and bi-modal distributions of equivalence ratio for a given set of values of ϕ' and the Taylor micro-scale l_ϕ of equivalence ratio variation. The Taylor micro-scale l_ϕ of the equivalence ratio variation is defined as (Eswaran and Pope, 1988):

$$l\phi = \sqrt{\frac{6\langle[\phi - \langle\phi\rangle]^2\rangle}{\langle\nabla[\phi - \langle\phi\rangle]\cdot\nabla[\phi - \langle\phi\rangle]\rangle}} \tag{1}$$

where the angle bracket indicates the global mean evaluated over the whole of computational domain. The main objectives of the present study are:

(1) to demonstrate the influences of initial mixture inhomogeneity distribution on localized forced ignition and early stages of combustion for globally stoichiometric mixtures; and
(2) to provide physical explanations for the observed mixture distribution, u', ϕ', and l_ϕ dependences of the extent of burning following successful localized forced ignition of stratified mixtures.

The remainder of the article will be organized as follows. The information related to mathematical background and numerical implementation pertaining to the current analysis will be presented in the next section. This will be followed by the presentation of the results and subsequent discussion. The main findings will be summarized and conclusions will be drawn in the final section of this article.

Mathematical background and numerical implementation

It is extremely expensive to carry out detailed chemistry 3D DNS simulations for an extensive parametric analysis (Chen et al., 2009), as done in the current study. Thus, a modified single step chemical mechanism (Tarrazo et al., 2006) has been considered here:

$$\text{Fuel} + s\cdot\text{Oxidizer} \rightarrow (1+s)\,\text{Products} \tag{2}$$

where s indicates the mass of oxidizer consumed per unit mass of fuel consumption under stoichiometric conditions and the fuel reaction rate is given by an Arrhenius-type expression (Chakraborty et al., 2007, 2010; Chakraborty and Mastorakos, 2008; Mastorakos et al., 1997; Tarrazo et al., 2006; Wandel, 2013, 2014; Wandel et al., 2009):

$$\dot{w}_F = -\rho B^* Y_F Y_O \exp\left[\frac{-\beta(1-T)}{1-\alpha(1-T)}\right] \tag{3}$$

where Y_F and Y_O are the local fuel and oxidizer mass fractions respectively, ρ is the gas density and $T = \left(\hat{T} - T_0\right)/\left(T_{ad(\phi=1)} - T_0\right)$ is the nondimensional temperature, with $\hat{T}$, T_0, and $T_{ad(\phi=1)}$ being the instantaneous dimensional temperature, unburned gas temperature, and the adiabatic flame temperature of the stoichiometric mixture, respectively.

In Eq. (3), $\beta = \left(T_{ac}\left\{T_{ad(\phi=1)} - T_0\right\}\right)/\left(T^2_{ad(\phi=1)}\right)$ is the Zel'dovich number, $\alpha = \left(T_{ad(\phi=1)} - T_0\right)/T_{ad(\phi=1)}$ is a heat release parameter, and B^* is the normalized pre-exponential factor. The Zel'dovich number β is expressed as $\beta = 6f(\phi)$, where $f(\phi)$ is given by (Tarrazo et al., 2006):

$$f(\phi) = \begin{cases} 1 + 8.25(\phi - 1)^2 & \text{for} \quad \phi \leq 0.64 \\ 1 + 1.443(\phi - 1.07)^2 & \text{for} \quad \phi \geq 1.07 \\ 1.0 & \text{for} \quad 0.64 < \phi < 1.07 \end{cases} \tag{4}$$

The heat release per unit mass of fuel $H_\phi = \left[\left(T_{ad(\phi)} - T_0\right)C_P\right]/\left[Y_{F0(\phi)} - Y_{Fb(\phi)}\right]$ is given by: $H_\phi/H_{\phi=1} = 1.0$ for $\phi \leq 1$ and $H_\phi/H_{\phi=1} = 1.0 - \alpha_H(\phi - 1)$ for $\phi > 1$ (Tarrazo et al., 2006), where $\alpha_H = 0.21$ and $Y_{F0(\phi)}$ and $Y_{Fb(\phi)}$ are the fuel mass fraction in the unburned and fully burned gas, respectively, for a premixed flame of equivalence ratio . The equivalence ratio dependence of β and H_ϕ enables the single step chemical mechanism given by Eq. (2) to mimic the realistic equivalence ratio dependence of the unstrained laminar burning velocity $S_{b(\phi)}$ (Tarrazo et al., 2006) obtained from experimental measurements (Egolfopoulos et al., 1989). The Lewis numbers of all species are taken to be unity for the current analysis. The combustion is assumed to take place in the gaseous phase where all the species are considered to be perfect gases. The mixture inhomogeneity in stratified mixtures is often characterized in terms of mixture fraction ξ, which can be expressed in terms of both fuel and oxidizer mass fractions (i.e., Y_F and Y_O) as: $\xi = (Y_F - Y_O/s + Y_{O\infty}/s)/(Y_{F\infty} + Y_{O\infty}/s)$ (Bilger, 1988) where $Y_{F\infty}$ is the fuel mass fraction in the pure fuel stream and $Y_{O\infty}$ is the oxidizer mass fraction in air. The equivalence ratio ϕ can be expressed in terms of mixture fraction ξ and the stoichiometric mixture fraction ξ_{st} as: $\phi = (1 - \xi_{st})\xi/(1 - \xi)\xi_{st}$ where $\xi_{st} = Y_{O\infty}/(sY_{F\infty} + Y_{O\infty})$. For the present analysis, $s = 4$, $Y_{F\infty} = 1.0$, and $Y_{O\infty} = 0.233$ have been taken, which yields $Y_{Fst} = 0.055$ and $\xi_{st} = 0.055$. These values represent methane-air mixtures. The extent of the completion of the chemical reaction can be characterized by a reaction progress variable c, which is defined as (Chakraborty et al., 2007; Chakraborty and Mastorakos, 2008; Hélie and Trouvé, 1998; Malkeson and Chakraborty, 2010; Patel and Chakraborty, 2014):

$$c = \frac{(\xi Y_{F\infty} - Y_F)}{\left(\xi Y_{F\infty} - \max\left[0, \left(\frac{\xi - \xi_{st}}{1 - \xi_{st}}\right)\right] Y_{F\infty}\right)} \tag{5}$$

According to this equation, c rises monotonically from 0 in the fully unburned reactants to 1.0 in the fully burned products.

The heat addition by the ignitor is accounted for by a source term q''' in the energy conservation equation (Chakraborty et al., 2007; Chakraborty and Mastorakos, 2008; Neophytou et al., 2010; Patel and Chakraborty, 2014):

$$\frac{\partial}{\partial t}\rho E + \frac{\partial}{\partial x_k}\rho u_k E = -\frac{\partial}{\partial x_k}u_k P + \frac{\partial}{\partial x_k}\tau_{ki}u_i + \frac{\partial}{\partial x_k}\left[\frac{\lambda \partial \hat{T}}{\partial x_k}\right] - \frac{\partial}{\partial x_i}\rho \sum_N^{k=1} h_{s,k}Y_k V_{k,i} + \dot{w}_T + q''' \tag{6}$$

It is worth noting that in Eq. (6) the term $\frac{\partial}{\partial x_i}\rho \sum_N^{k=1} h_{s,k}Y_k V_{k,i} = C_P(T - T_0)\sum_N^{k=1} h_k V_{k,i} = 0$ for the present analysis as the specific heats at constant pressure and volume are taken to be constant

and the same for all of the species. In Eq. (6), $h_{s,k}$ is the specific enthalpy, P is the pressure, τ_{ki} is the viscous shear stress, $\dot{w}_T = |\dot{w}_F| H_\phi$ is the source term originating from heat release due to combustion, and $E = \int_{\hat{T}}^{T_{ref}} C_V d\dot{T} + u_k u_k/2$ is the specific stagnation internal energy.

The source term q''' in Eq. (6) is assumed to follow a Gaussian distribution in the radial direction from the center of the ignitor (Chakraborty et al., 2007; Chakraborty and Mastorakos, 2008; Espi and Liñán, 2001, 2002; Neophytou et al., 2010; Patel and Chakraborty, 2014; Wandel, 2013, 2014; Wandel et al., 2009) and is expressed in the following manner: $q'''(r) = A_q \exp(-r^2/2R^2)$, where r is the radial direction from the center of the ignitor and R is the characteristic width of energy deposition, which is taken to be $R = 1.10 l_f$, where $l_f = D_0/S_{b(\phi=1)}$ is the Zel'dovich flame thickness of the stoichiometric mixture with D_0 and $S_{b(\phi=1)}$ being the unburned gas diffusivity and the unstrained laminar burning velocity of the stoichiometric mixture, respectively. The constant A_q is determined by the volume integration $\dot{Q} = \int_V q''' dV$, where $\dot{Q}$ is the ignition power, which is defined as: $\dot{Q} = a_{sp}\rho_0 C_P \tau T_0 \left(4\pi l_f^3/3\right)\left[\left\{H_1(t) - H_2\left(t - t_{sp}\right)\right\}/t_{sp}\right]$, where a_{sp} is a parameter that determines the total energy deposited by the ignitor and is taken to be $a_{sp} = 3.6$ in the current analysis following previous studies (Chakraborty et al., 2007; Chakraborty and Mastorakos, 2008; Patel and Chakraborty, 2014). The energy deposition duration t_{sp} is expressed as: $t_{sp} = b_{sp} t_f$, where b_{sp} is the energy deposition duration parameter and t_f is a characteristic chemical timescale given by: $t_f = l_f/S_{b(\phi=1)}$. The parameter b_{sp} for optimum spark duration varies between $0.2 < b_{sp} < 0.4$ (Ballal and Lefebvre, 1977b) and $b_{sp} = 0.2$ has been taken for the current analysis following previous studies (Chakraborty et al., 2007; Chakraborty and Mastorakos, 2008; Patel and Chakraborty, 2014; Wandel, 2013, 2014; Wandel et al., 2009). The details of spark formation (momentum modification contribution, plasma formation, and shock wave) are kept beyond the scope of the present analysis in order to keep this study computationally feasible. The pseudo-spectral methods proposed by Eswaran and Pope (1988) and Rogallo (1981) were used for generating initial ϕ fields following bi-modal and Gaussian distributions, respectively. The pseudo-spectral method proposed by Rogallo (1981) is also used to produce a homogeneous isotropic incompressible velocity field to initialize turbulent velocity fluctuations according to the Batchelor–Townsend spectrum (Batchelor and Townsend, 1948). For the current analysis, a globally stoichiometric (i.e., $\langle\phi\rangle = 1.0$) mixture has been considered. The initial magnitudes of the normalized rms value of turbulent velocity $u'/S_{b(\phi=1)}$, rms value of equivalence ratio ϕ', and normalized Taylor micro-scale of equivalence ratio variation l_ϕ/l_f are listed in Table 1. The ratio of longitudinal integral length scale to flame thickness is considered to be $L_{11}/l_f = 3.36$ for all turbulent cases following previous analyses (Chakraborty et al., 2007; Chakraborty and Mastorakos, 2008; Neophytou et al., 2010; Patel and Chakraborty, 2014; Wandel, 2013, 2014; Wandel et al., 2009). The case names are chosen in such a manner so that G and B stand for initial Gaussian and bi-modal equivalence ratio ϕ distributions; T0, T4, and T6 indicate increasing turbulence intensity $u'/S_{b(\phi=1)}$; X, Y, and Z indicate increasing values of ϕ'; and D, E, and F denote increasing values of l_ϕ/l_f (e.g., GYT6F corresponds to a case with initial Gaussian ϕ distribution with initial values of $\phi' = 0.4; u'/S_{b(\phi=1)} = 6.0; l\phi/l_f = 8.3$). The initial mixture

Table 1. Initial values of the simulation parameters.

	$\phi' = 0.2$ [X]			$\phi' = 0.4$ [Y]			$\phi' = 0.6$ [Z]		
$\frac{L_{11}}{l_f} = 3.36$	$\frac{u'}{S_{b(\phi=1)}} = 0$ [T0]	$\frac{u'}{S_{b(\phi=1)}} = 4$ [T4]	$\frac{u'}{S_{b(\phi=1)}} = 6$ [T6]	$\frac{u'}{S_{b(\phi=1)}} = 0$ [T0]	$\frac{u'}{S_{b(\phi=1)}} = 4$ [T4]	$\frac{u'}{S_{b(\phi=1)}} = 6$ [T6]	$\frac{u'}{S_{b(\phi=1)}} = 0$ [T0]	$\frac{u'}{S_{b(\phi=1)}} = 4$ [T4]	$\frac{u'}{S_{b(\phi=1)}} = 6$ [T6]
$l_\phi/l_f = 2.1$	GT0XD	GT4XD	GT6XD	GT0YD	GT4YD	GT6YD	GT0ZD	GT4ZD	GT6ZD
[D]	BT0XD	BT4XD	BT6XD	BT0YD	BT4YD	BT6YD	BT0ZD	BT4ZD	BT6ZD
$l_\phi/l_f = 5.5$	GT0XE	GT4XE	GT6XE	GT0YE	GT4YE	GT6YE	GT0ZE	GT4ZE	GT6ZE
[E]	BT0XE	BT4XE	BT6XE	BT0YE	BT4YE	BT6YE	BT0ZE	BT4ZE	BT6ZE
$l_\phi/l_f = 8.3$	GT0XF	GT4XF	GT6XF	GT0YF	GT4YF	GT6YF	GT0ZF	GT4ZF	GT6ZF
[F]	BT0XF	BT4XF	BT6XF	BT0YF	BT4YF	BT6YF	BT0ZF	BT4ZF	BT6ZF

Note. [G]: Gaussian; [B]: Bi-modal distribution. Homogeneous cases: T0, T4, T6.

distributions for $\phi' = 0.4$ with different values of l_ϕ/l_f are shown in Figure 1, which indicates that the clouds of mixture inhomogeneities increase in size with increasing l_ϕ/l_f.

A compressible 3D DNS code SENGA (Chakraborty et al., 2007; Chakraborty and Mastorakos, 2008; Neophytou et al., 2010; Patel and Chakraborty, 2014, Wandel, 2013, 2014; Wandel et al., 2009) was used to carry out the simulations in a domain of size $33l_f \times 33l_f \times 33l_f$, which ensures that about 10 integral eddies are retained on each side of the domain. The simulation domain is discretized by a Cartesian grid of size $200 \times 200 \times 200$ with uniform grid spacing Δx. This grid spacing ensures 10 grid points within the thermal flame thickness $\delta_{th(\phi=1)} = \left[T_{ad(\phi=1)} - T_0\right]/\max\left|\nabla \hat{T}\right|_L$ of the stoichiometric mixture, which ensures $\eta > \Delta x$, where η is the Kolmogorov length scale. The boundaries in

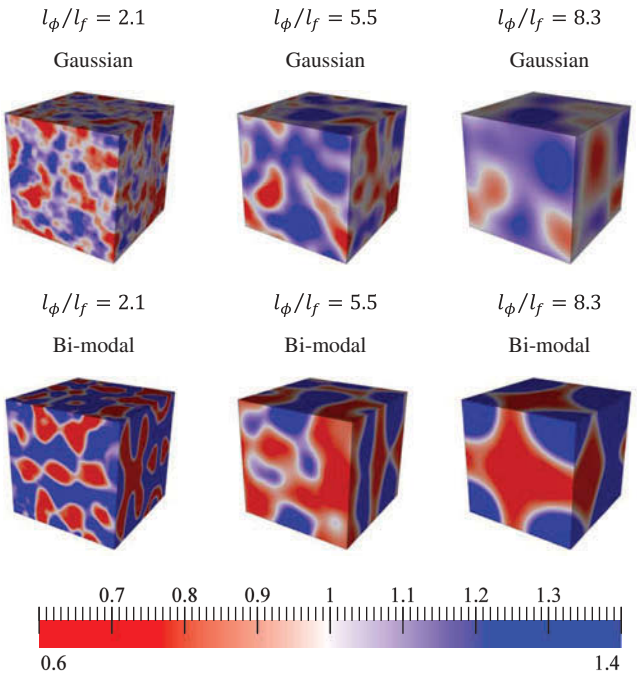

Figure 1. Initial $\phi' = 0.4$ Gaussian (1st row) and bi-modal (2nd row) distribution cases for different values of l_ϕ/l_f.

the x_1-direction are taken to be partially nonreflecting and are specified using the Navier–Stokes characteristic boundary conditions (NSCBC) technique (Poinsot and Lele, 1992), whereas the boundaries in the other directions are considered to be periodic. A 10th-order central difference scheme is used for spatial differentiation for the internal grid points, and the order of differentiation gradually reduces to a one-sided 2nd-order scheme at the nonperiodic boundaries. The time advancement is carried out using a third order low-storage Runge–Kutta scheme (Wray, 1990). Four different realizations of both initial (Gaussian and bi-modal) mixture distributions spanning 27 different parameters have been considered here, which amounts to 219 simulations altogether ($27 \times 4 \times 2 = 216$ stratified mixtures cases $+ 3$ homogeneous mixture cases). For the present analysis, flame-turbulence takes place under decaying turbulence. The DNS simulations under decaying turbulence should be carried out for a time $t_{sim} \geq \max(t_e, t_f)$, where $t_e = L_{11}/\sqrt{k}$ is the initial eddy turnover time with k being the initial turbulent kinetic energy. Statistics for all cases are presented at $t = 8.40t_{sp} = 1.68t_f$, which corresponds to about $2t_e$ and $3t_e$ for the initial values of $u'/S_{b(\phi=1)} = 4.0$ and $u'/S_{b(\phi=1)} = 6.0$, respectively. The simulation time used in the current analysis is comparable to that used in several analyses, which contributed to the fundamental physical understanding of localized forced ignition in the past (Chakraborty et al., 2007; Chakraborty and Mastorakos, 2008; Neophytou et al., 2010; Patel and Chakraborty, 2014, Wandel, 2013, 2014; Wandel et al., 2009; Yu and Bai, 2013).

Results and discussion

The temporal evolution of the nondimensional maximum temperature (i.e., $T_{\max} = (\hat{T}_{\max} - T_0)/(T_{ad(\phi=1)} - T_0)$ and the normalized maximum fuel reaction rate magnitude (i.e., $(\dot{\Omega}_F)_{\max} = |\dot{w}_F|_{\max} \times l_f/\rho_0 S_{b(\phi=1)}$) for the initial Gaussian and bi-modal distributions are shown in Figures 2 and 3, respectively. It can be seen from Figures 2 and 3 that $T_{\max}$ rises with time due to energy deposition during $0<t<t_{sp}$, which eventually gives rise to a thermal runaway once $T_{\max}$ attains a value close to $T_c \approx 1 - 1/\beta_{\phi=1}$, leading to rapid increases in $T_{\max}$ and $(\dot{\Omega}_F)_{\max}$ with time. The high thermal gradient between the hot gas kernel and the surrounding unburned gas leads to a high rate of heat transfer from the ignition kernel. This, in turn, leads to decreases in $T_{\max}$ and $(\dot{\Omega}_F)_{\max}$ with time once the ignitor is switched off, but $T_{\max}$ ultimately settles to the nondimensional adiabatic flame temperature of the stoichiometric mixtures (i.e., $T \approx 1.0$) and $(\dot{\Omega}_F)_{\max}$ settles to a much smaller value, which no longer changes appreciably with time for $t \gg t_{sp}$ in the cases where self-sustained combustion is obtained following successful ignition.

A comparison between Figures 2 and 3 shows that self-sustained combustion has been obtained for all Gaussian distribution cases with $u'/S_{b(\phi=1)} = 0.0$ and 4.0, whereas some cases with initial bi-modal distribution (e.g., BT4YE and BT4ZE) fail to achieve self-sustained combustion for $u'/S_{b(\phi=1)} = 4.0$. It has been found that the bi-modal distribution cases with initial $l_\phi/l_f = 5.5$ are more prone to flame extinction at $t > t_{sp}$ than the initial $l_\phi/l_f = 2.1$ and 8.3 cases for initial $\phi' = 0.4$ and 0.6, but no such trend is observed for the corresponding cases with initial Gaussian equivalence ratio distribution. By

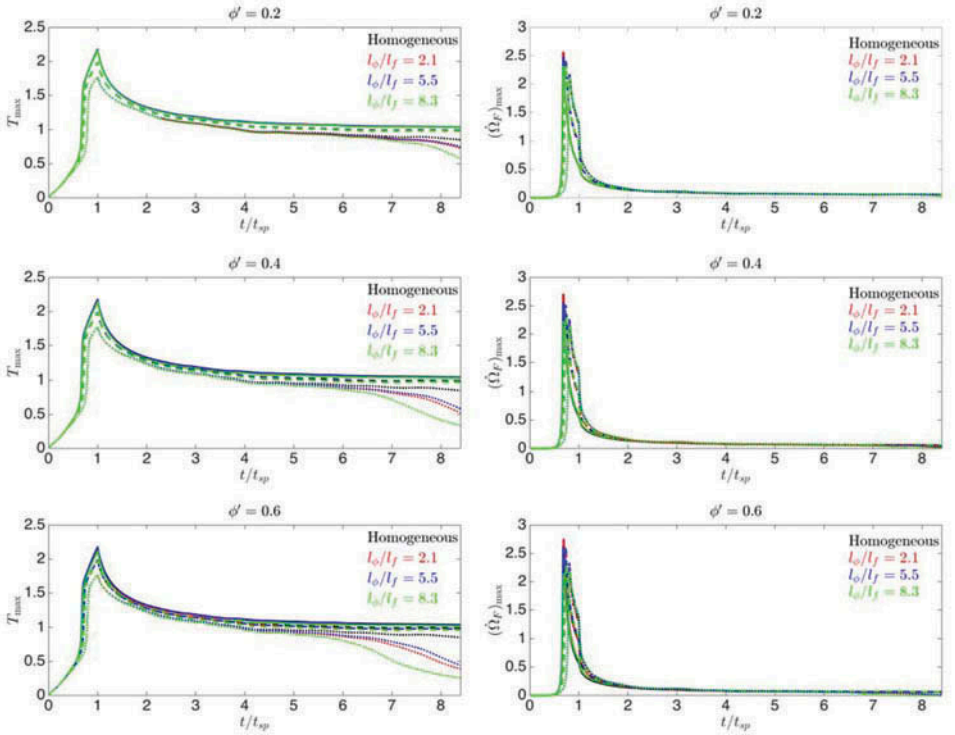

Figure 2. Temporal evolution of the maximum values of nondimensional temperature $T_{\max} = \left(\hat{T}_{\max} - T_0\right)/\left(T_{ad(\phi=1)} - T_0\right)$ and normalized fuel reaction rate magnitude $(\dot{\Omega}_F)_{max} = |\dot{w}_F|_{max} \times l_f/\rho_0 S_{b(\phi=1)}$ for all cases with initial Gaussian mixture distributions from Table 1 (with $u'/S_{b(\phi=1)} =$ 0.0: ———, $u'/S_{b(\phi=1)}$= 4.0: — — —; $u'/S_{b(\phi=1)}$ = 6.0: - - - -).

contrast, some cases with initial bi-modal distribution show more resistance to flame extinction at $t > t_{sp}$ for initial $u'/S_{b(\phi=1)} =$ 6.0 (e.g., the initial bi-modal distribution cases BT6XD, BT6XE, BT6XF, and BT6YF exhibit self-sustained combustion) than the corresponding cases with initial Gaussian distribution (all cases with initial Gaussian distribution fail to achieve self-sustained combustion for initial $u'/S_{b(\phi=1)} =$ 6.0). In general, the probability of flame extinction at $t > t_{sp}$ (i.e., without any external addition of energy) increases with increasing $u'/S_{b(\phi=1)}$ for both initial bi-modal and Gaussian distribution cases. The observations made from Figures 2 and 3 indicate that the nature of initial mixture distribution, $u'/S_{b(\phi=1)}$, ϕ', and l_ϕ/l_f, have important influences on the possibility of obtaining self-sustained combustion following successful ignition in stratified mixtures.

The distributions of fuel mass fraction (i.e., Y_F), nondimensional temperature (i.e., T), normalized fuel reaction rate magnitude (i.e., $\dot{\Omega}_F = |\dot{w}_F| \times l_f/\rho_0 S_{b(\phi=1)}$), and equivalence ratio ϕ at $t = 1.05t_{sp}$ and $t = 8.40t_{sp}$ at the central $x_1 - x_2$ plane for the cases GT4YD and BT4YD are shown in Figure 4. Similar qualitative behavior has been observed for other cases but the burned gas volume has been found to decrease with increasing $u'/S_{b(\phi=1)}$ irrespective of the nature of the initial mixture distribution. The contours of T remain

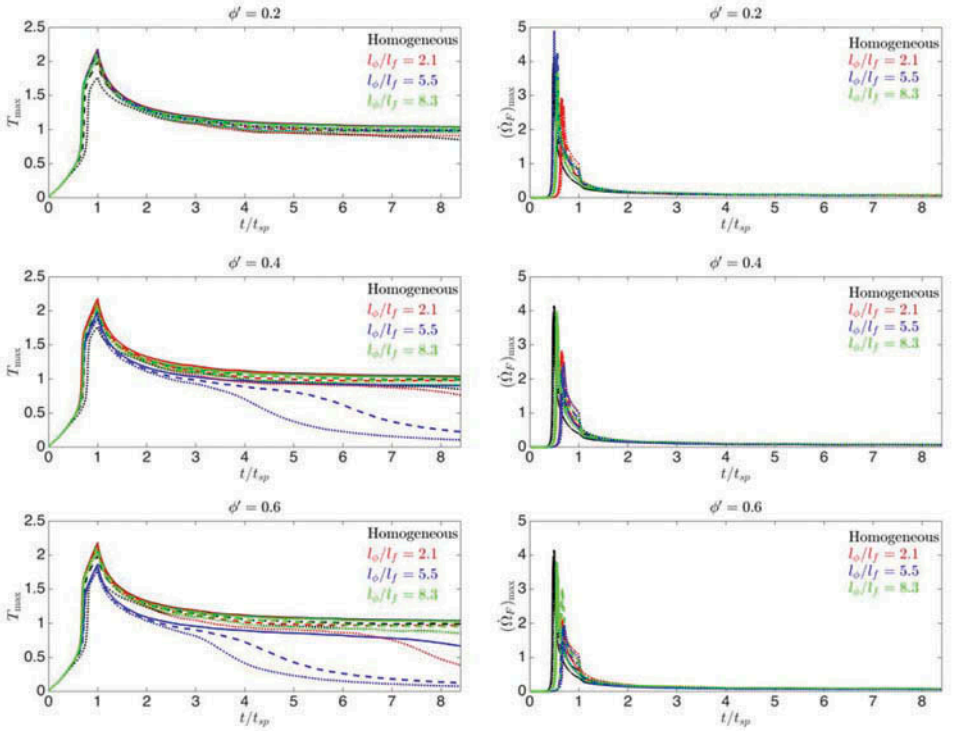

Figure 3. Temporal evolution of the maximum values of nondimensional temperature $T_{\max} = \left(\hat{T}_{\max} - T_0\right)/\left(T_{ad(\phi=1)} - T_0\right)$ and normalized fuel reaction rate magnitude $(\dot{\Omega}_F)\max = |\dot{w}_F|_{\max} \times l_f/\rho_0 S_{b(\phi=1)}$ for all cases with initial bi-modal mixture distributions from Table 1 (with $u'/S_{b(\phi=1)} =$ 0.0: ———, $u'/S_{b(\phi=1)}$ = 4.0: — — —; $u'/S_{b(\phi=1)}$ = 6.0: - - - -).

approximately spherical during the period of energy deposition but they become increasingly wrinkled as time progresses for all turbulent cases. The evolution of T contours is principally determined by the diffusion of deposited energy during $0<t<t_{sp}$, whereas after ignition the evolution of isotherms depends on the magnitude of the reaction rate at the local mixture composition and the flame stretch induced by the background fluid motion. The stretch rate dependencies of local flame propagation are found to be qualitatively similar to those reported earlier by Malkeson and Chakraborty (2010) and thus are not repeated here for the sake of brevity. Additionally, it can be seen from Figure 4 that the level of nonuniformity of ϕ decreases as time progresses in all cases. The evolution of the mixing process can be illustrated by the temporal evolution of the pdfs of ϕ, which is shown in Figure 5. The cases with an initial Gaussian distribution exhibit higher probabilities of finding $\phi \approx \langle\phi\rangle = 1.0$ than the corresponding cases with an initial bi-modal distribution. The equivalence ratio pdfs for the initial Gaussian distribution cases show peak values at $\phi \approx \langle\phi\rangle = 1.0$, whereas the cases with initial bi-modal distribution show higher probabilities of finding $\phi < \langle\phi\rangle$ and $\phi > \langle\phi\rangle$ than the initial Gaussian distribution cases. Figure 5 shows that the pdf of ϕ for the initial bi-modal distribution cases approaches an approximate Gaussian distribution as time progresses due to mixing,

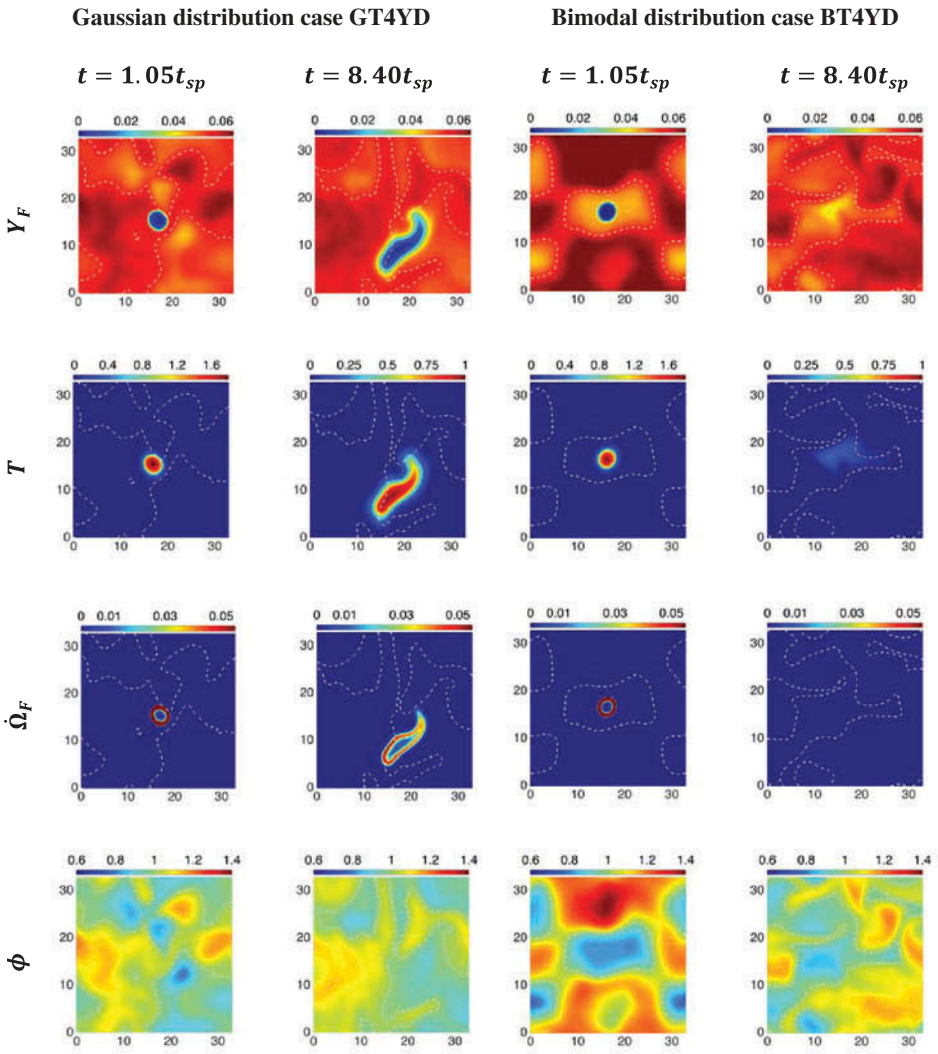

Figure 4. Distribution of mass fraction (i.e., Y_F—1st row), nondimensional temperature (i.e., T—2nd row), normalized fuel reaction rate magnitude (i.e., $\dot{\Omega}_F = |\dot{w}_F| \times l_f/\rho_0 S_{b(\phi=1)}$—3rd row), and equivalence ratio (i.e., ϕ—4th row) at $t = 1.05t_{sp}$ and $t = 8.40t_{sp}$ at the central $x_1 - x_2$ plane for the cases GT4YD (columns 1 and 2) and BT4YD (columns 3 and 4). The white broken line shows the stoichiometric mixture fraction $\xi = \xi_{st}$.

whereas the width of ϕ pdf decreases, and the peak value of ϕ pdf at $\phi \approx \langle\phi\rangle = 1.0$ increases with time in the initial Gaussian distribution cases. A comparison between the equivalence ratio pdfs between the initial bi-modal and Gaussian distribution cases reveals that the probability of finding $\phi \approx 1.0$ ($\phi \neq 1.0$) is greater for the cases with initial Gaussian (bi-modal) distribution than those with initial bi-modal (Gaussian) distribution for a given set of values of ϕ' and l_ϕ/l_f. It can further be seen from Figure 5 that the effects of mixing are stronger for smaller values of l_ϕ/l_f for a given value of $u'/S_{b(\phi=1)}$, as the mean scalar dissipation rate $N_\xi = D\nabla\xi \cdot \nabla\xi$ of mixture fraction scales as $\langle N_\xi\rangle \sim D\xi'^2/l_\phi^2$,

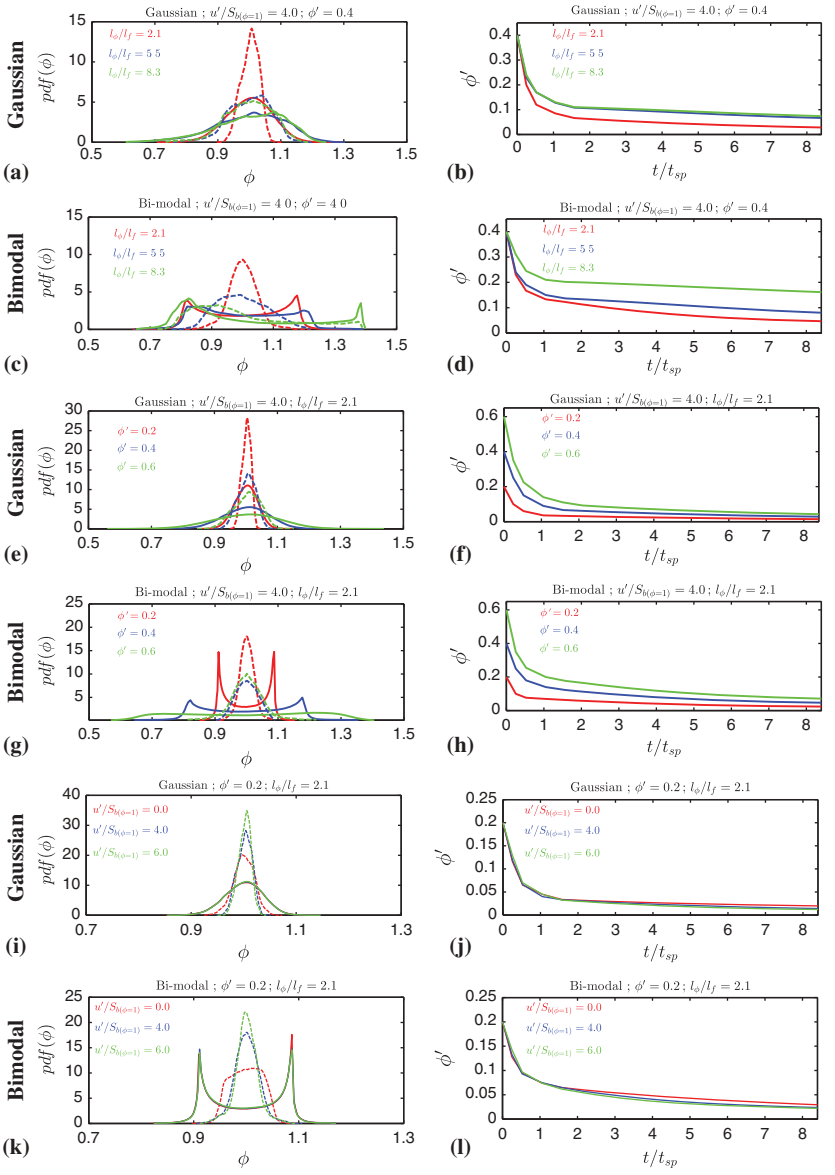

Figure 5. Temporal evolution of the pdf of equivalence ratio ϕ (1st row) at $t = 1.05t_{sp}$ (solid line) and $t = 8.40t_{sp}$ (broken line) (1st column) and temporal evolution of rms value of equivalence ratio ϕ' (2nd column) evaluated over the whole domain for a selection of cases: (a–d) effects of initial l_ϕ/l_f for cases with initial $\phi' = 0.4$ and $u'/S_{b(\phi=1)} = 4.0$; (e–h) effects of initial ϕ' for cases with initial $u'/S_{b(\phi=1)} = 4.0$ and $l_\phi/l_f = 2.1$; (i–l) effects of initial $u'/S_{b(\phi=1)}$ for cases with initial $\phi' = 0.2$ and $l_\phi/l_f = 2.1$.

where ξ' is the rms value of mixture fraction. This suggests that N_ξ is likely to assume high magnitudes for small values of l_ϕ/l_f for a given value of ξ'. This behavior can be confirmed from the temporal evolution of ϕ' shown in Figure 5, which demonstrates that the high rate of mixing (i.e., rapid decay rate of ϕ') is associated with small values of l_ϕ/l_f and vice versa. Furthermore, the probability of finding high values of N_ξ increases with increasing

$u'/S_{b(\phi=1)}$, as turbulent straining acts to generate scalar gradient (Vedula et al., 2001), which in turn increases the rate of micro-mixing. This is consistent with high decay rate of ϕ' for high values of $u'/S_{b(\phi=1)}$ (see Figure 5).

It is vital to understand the flame structure originating from localized forced ignition to explain the observed burning behavior for different mixture distributions. The mode of combustion can be characterized by the flame index $I_c = \nabla Y_F \cdot \nabla Y_O/(|\nabla Y_F||\nabla Y_O|)$, which assumes positive (negative) values for premixed (non-premixed) mode of combustion (Hélie and Trouvé, 1998; Yamashita et al., 1996). The percentage of overall heat release arising from premixed (i.e., $I_c > 0$) and non-premixed (i.e., $I_c < 0$) modes of combustion at $t = 8.40t_{sp}$ are shown in Figure 6 for a selection of cases. It is evident from Figure 6 that the chemical reaction takes place predominantly in premixed mode but some pockets of non-premixed combustion can also be found. Moreover, Figure 6 shows that the percentage of heat release from the premixed mode of combustion is greater in the initial Gaussian mixture distribution cases in comparison to the initial bi-modal distribution cases. This is consistent with higher probability of finding $\phi \approx \langle\phi\rangle$ in the initial Gaussian mixture distribution cases than in the cases with initial bi-modal distribution, as shown in Figure 5. The percentage of heat release arising from the non-premixed mode of combustion increases with increasing ϕ' for both types of initial mixture distributions, but this effect is more prominent in the initial bi-modal distribution cases in comparison to the initial Gaussian distribution cases. Furthermore, the percentage of heat release arising from non-premixed combustion (i.e., $I_c < 0$) decreases with decreasing (increasing) values of l_ϕ/l_f (u') for a given value of ϕ', as a result of improved mixing due to high magnitudes of N_ξ, and this effect is more prominent in the initial bi-modal distribution cases than in the initial Gaussian distribution cases (see Figure 6c).

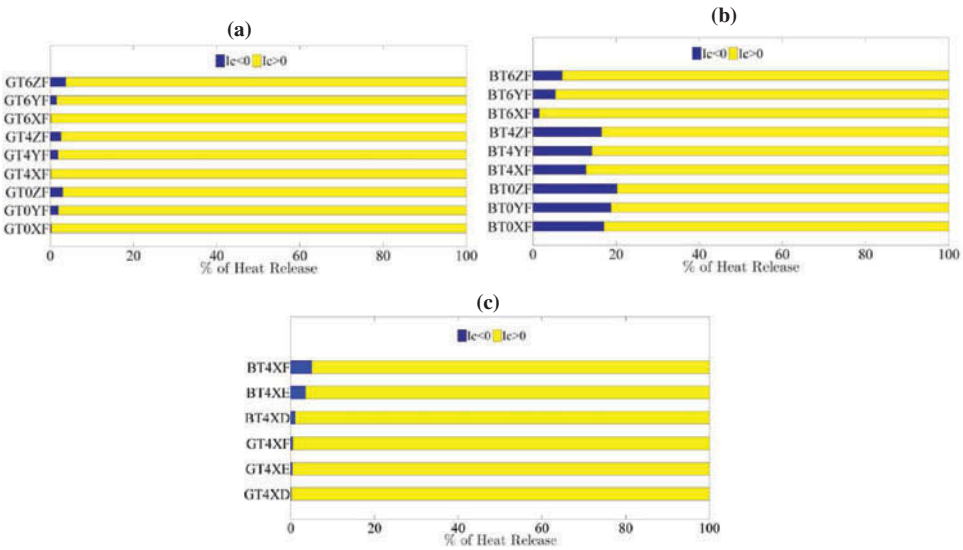

Figure 6. Percentage of overall heat release arising from premixed ($I_c > 0$) and non-premixed ($I_c < 0$) combustion at $t = 8.40t_{sp}$ for a selection of cases: effects of initial values of ϕ' and $u'/S_{b(\phi=1)}$ for (a) Gaussian and (b) bi-modal distributions of equivalence ratio with initial $l_\phi/l_f = 8.3$; (c) effects of initial l_ϕ/l_f for cases with initial $\phi' = 0.2$ and $u'/S_{b(\phi=1)} = 4.0$.

It is important to understand the reaction zone structure of the flames initiated by the localized forced ignition, in order to explain the effects of stratification on the extent of burning following successful ignition. The scatter of $\dot{\Omega}_F = |\dot{w}_F| \times l_f/\rho_0 S_{b(\phi=1)}$ with reaction progress variable c is presented in Figure 7a at $t = 8.40t_{sp}$ for the case GT4YF and a similar qualitative behavior has been observed for all cases, including the initial bi-modal distribution cases (Patel and Chakraborty, 2014), where the self-sustained combustion has been obtained. Figure 7a shows that the high values of $\dot{\Omega}_F$ are obtained close to $c = 0.8$, which is consistent with reaction rate profiles obtained from previous analyses (Chakraborty et al., 2007, 2010; Chakraborty and Mastorakos, 2008; Patel and Chakraborty, 2014). The scatter of $\dot{\Omega}_F$ with mixture fraction ξ for the case GT4YF is presented in Figure 7b, which shows that a considerable amount of scatter, and the same qualitative behavior is observed for other cases including the initial bi-modal distribution cases (Patel and Chakraborty, 2014). The large variation of nondimensional temperature T on a given ξ isosurface (due to both unburned and burned contributions)

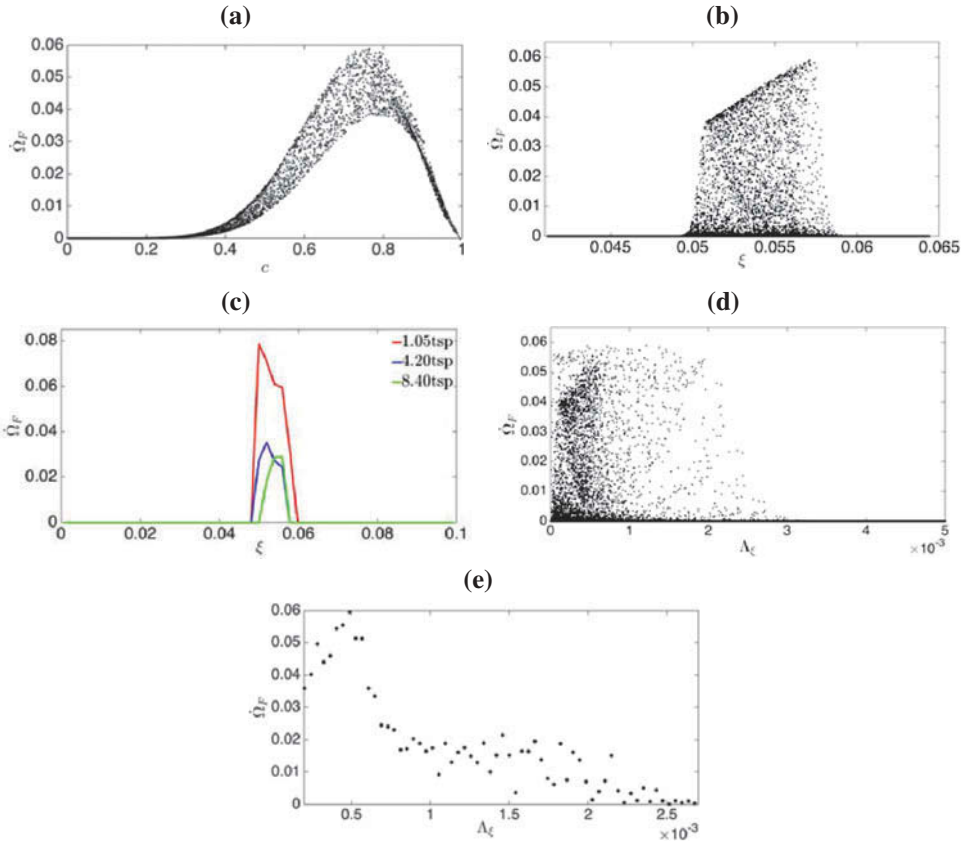

Figure 7. (a) Scatter of the normalized fuel reaction rate magnitude $\dot{\Omega}_F = |\dot{w}_F| \times l_f/\rho_0 S_{b(\phi=1)}$ with reaction progress variable c, (b) scatter of $\dot{\Omega}_F$ with mixture fraction ξ, (c) variation of the mean values of $\dot{\Omega}_F$ conditional on mixture fraction ξ for reaction progress variable range $0.5 \leq c \leq 0.9$, (d) scatter of $\dot{\Omega}_F$ with normalized scalar dissipation rate $\Lambda_\xi = N_\xi t_f/\xi_{st}^2(1-\xi_{st})^2$, (e) variation of the mean values of $\dot{\Omega}_F$ conditional on normalized scalar dissipation rate Λ_ξ for the progress variable range $0.7 \leq c \leq 0.9$. All variation are shown for the case GT4YF.

leads to a large extent of scatter of $\dot{\Omega}_F$. Furthermore, Figure 7b shows that the high values of $\dot{\Omega}_F$ are obtained towards the slightly rich side (i.e., $\xi \approx 0.06$), which corresponds to $\phi \approx 1.10$, where the unstrained planar laminar burning velocity attains its maximum value (Egolfopoulos et al., 1989; Tarrazo et al., 2006). The temporal evolution of the mean values of $\dot{\Omega}_F$ conditional of mixture fraction ξ in the region corresponding to $0.5 \leq c \leq 0.9$ (i.e., where the high values of reaction rate magnitudes are obtained; see Figure 7a) for the case GT4YF is shown in Figure 7c for different time instants. Figure 7c demonstrates that the temperature distribution remains qualitatively similar following successful ignition and the same qualitative behavior has been observed for other cases. In stratified mixture combustion, the scalar dissipation rate of mixture fraction $N_\xi = D\nabla\xi\cdot\nabla\xi$ also affects the reaction zone structure (Chakraborty et al., 2007, 2010; Chakraborty and Mastorakos, 2008; Im et al., 1998; Mastorakos et al., 1997; Patel and Chakraborty, 2014). The scatter of $\dot{\Omega}_F$ with varying normalized scalar dissipation rate $\Lambda_\xi = N_\xi t_f/\xi_{st}^2(1-\xi_{st})^2$ at $t = 8.40t_{sp}$ for the case GT4YF is shown in Figure 7d. Additionally, the mean values of $\dot{\Omega}_F$ conditional on the values for Λ_ξ in the most reactive region (i.e., $0.7 \leq c \leq 0.9$) is shown in Figure 7e for the case GT4YF. Figure 7e shows a predominant negative correlation between $\dot{\Omega}_F$ and Λ_ξ, which further indicates that $\dot{\Omega}_F$ attains relatively high values where combustion takes place predominantly in the premixed mode and thus high values of $\dot{\Omega}_F$ are associated with small values of Λ_ξ. A similar behavior is observed for all other initial Gaussian and bi-modal distribution cases, which is also consistent with previous findings (Chakraborty et al., 2007, 2010; Chakraborty and Mastorakos, 2008; Im et al., 1998; Mastorakos et al., 1997; Patel and Chakraborty, 2014) in the context of localized ignition.

The extent of burning can be characterized by the burned gas mass m_b with $c \geq 0.9$ (Chakraborty et al., 2007, 2010; Chakraborty and Mastorakos, 2008; Patel and Chakraborty, 2014; Wandel et al., 2009). The temporal evolution of the mean and standard deviations of burned gas mass normalized by the mass of an unburned gas sphere with a radius equal to l_f (i.e., $[4/3]\pi\rho_0 l_f^3$) for all cases with initial Gaussian and bi-modal distributions of equivalence ratio are shown in Figures 8 and 9, respectively. It is evident from Figures 8 and 9 that the mean value of $m_b(c \geq 0.9)$ decreases with increasing $u'/S_{b(\phi=1)}$ in both types of initial mixture distributions. An increase in u' leads to an increase in eddy diffusivity $D_t \sim u'L_{11}$ for a given value of L_{11}, which leads to a greater amount of heat loss from the hot gas kernel for high values of u'. The heat release due to combustion must overcome the heat loss in order to sustain combustion following successful ignition. The probability of findings high values of c decreases with increasing $u'/S_{b(\phi=1)}$ due to enhanced heat transfer rate from hot gas kernel for both types of initial mixture distributions. The smaller extent of burning rate for higher values of $u'/S_{b(\phi=1)}$ and the adverse effect of $u'/S_{b(\phi=1)}$ on the extent of burning are consistent with previous findings (Ballal and Lefebvre, 1977a; Chakraborty et al., 2007, 2010; Chakraborty and Mastorakos, 2008; Huang et al., 2007; Klein et al., 2008; Patel and Chakraborty, 2014; Poinsot et al., 1995). Furthermore, Figures 8 and 9 show that an increase in ϕ' leads to a decrease of the mean value of $m_b(c \geq 0.9)$irrespective of the nature of initial mixture distribution. The burning velocity of mixtures with $\phi < 1.0$ and $\phi > 1.10$ is smaller than that in the mixtures with $1.0 \leq \phi \leq 1.10$. The probability of finding $1.0 \leq \phi \leq 1.10$ decreases with increasing ϕ' and this gives rise to a reduction in burning rate for high

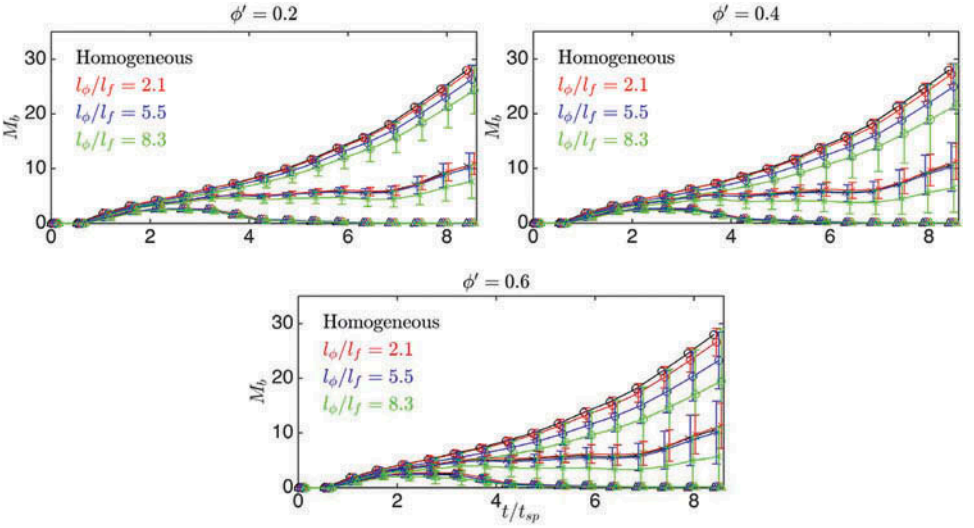

Figure 8. Temporal evolution of mean $M_b = [m_b(c \geq 0.9)]/\left[\{4/3\}\pi\rho_0 l_f^3\right]$ with standard deviation due to different realizations of initial conditions shown in the form of bars for all initial Gaussian mixture distribution cases with initial $u'/S_{b(\phi=1)} = 0.0$ [○], 4.0 [X], and 6.0 [Δ].

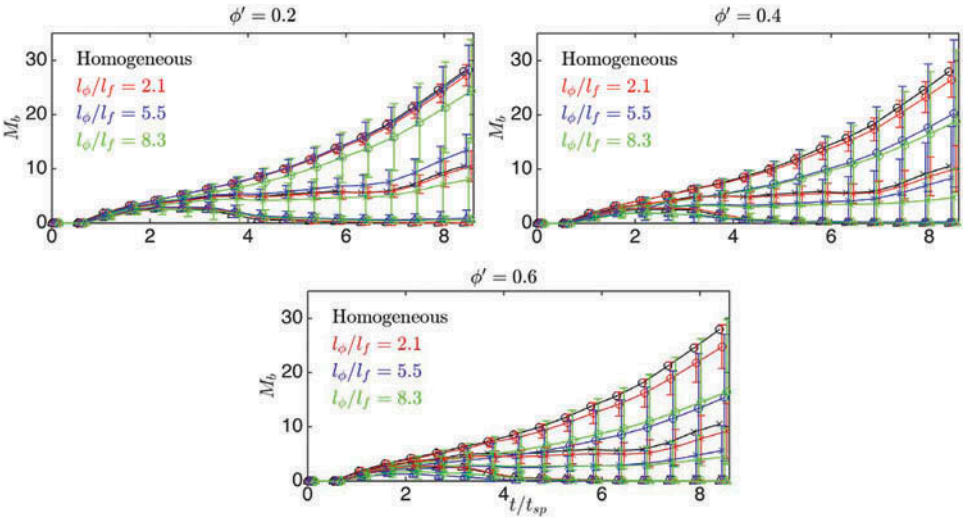

Figure 9. Temporal evolution of mean $M_b = [m_b(c \geq 0.9)]/\left[\{4/3\}\pi\rho_0 l_f^3\right]$ with standard deviation due to different realizations of initial conditions shown in the form of bars for all initial bi-modal mixture distribution cases with initial $u'/S_{b(\phi=1)} = 0.0$ [○], 4.0 [X], and 6.0 [Δ].

values of ϕ'. Additionally, Figures 8 and 9 indicate that increasing ϕ' for stratified cases increases the variability of burning irrespective of the nature of initial mixture distribution. The reduction in burning rate due to mixture stratification in globally stoichiometric mixtures is consistent with several previous analyses (Haworth et al., 2000; Jiménez et al., 2002; Malkeson and Chakraborty, 2010; Patel and Chakraborty, 2014; Renou et al., 2004; Samson, 2002; Zhou et al., 1998).

It is evident from Figures 8 and 9 that the mean values of $m_b(c \geq 0.9)$ remain comparable for the quiescent cases with initial $\phi' = 0.2$ for all values of l_ϕ/l_f in both initial bi-modal and Gaussian distributions. A comparison between Figures 8 and 9 indicates that the initial Gaussian mixture distribution cases with initial $u'/S_{b(\phi=1)} = 6.0$ fail to sustain combustion once the ignitor is switched off irrespective of the initial values of ϕ' and l_ϕ/l_f, whereas the initial bi-modal distribution cases with initial $\phi' = 0.2$ and $l_\phi/l_f = 5.5$ and 8.3 exhibit self-sustained combustion for initial $u'/S_{b(\phi=1)} = 6.0$. The bi-modal distribution cases show higher probability of finding $1.0 \leq \phi \leq 1.10$ than in the Gaussian distribution cases for $l_\phi/l_f > 2.1$ (see Figure 5). Thus, the heat release due to combustion for the initial bi-modal distribution cases with initial $\phi' = 0.2$ and $l_\phi/l_f = 5.5$ and 8.3 is greater than that in the corresponding Gaussian distribution cases and thus these initial bi-modal distribution cases show self-sustained combustion whereas flame extinction takes place for the initial Gaussian distribution cases at $t > t_{sp}$.

Among the bi-modal cases with initial $\phi' = 0.2$, the mean value of burned gas mass $m_b(c \geq 0.9)$ assumes the highest (lowest) magnitude for the cases with initial $l_\phi/l_f = 5.5$ ($l_\phi/l_f = 2.1$). By contrast, the mean value of burned gas mass $m_b(c \geq 0.9)$ assumes the highest (lowest) magnitude for the cases with initial $l_\phi/l_f = 8.3$ ($l_\phi/l_f = 5.5$) for initial $\phi' = 0.4$ and 0.6 in the initial bi-modal distribution cases. By contrast, the initial Gaussian distribution cases show an increase in the mean value of burned gas mass $m_b(c \geq 0.9)$with decreasing l_ϕ/l_f irrespective of initial ϕ'. The probability of finding highly reactive $1.0 \leq \phi \leq 1.10$ mixtures increases with decreasing l_ϕ/l_f, due to more efficient mixing for small values of l_ϕ for initial $\phi' = 0.4$ and 0.6 cases (see Figure 5). The probability of finding highly reactive mixture corresponding to $1.10 > \phi > 1.0$ is greater in the cases with initial values of $l_\phi/l_f = 5.5$ and 8.3 (the probability of finding $1.10 > \phi > 1.0$ is greater in the initial $l_\phi/l_f = 5.5$ cases than in the initial $l_\phi/l_f = 8.3$ cases) for initial $\phi' = 0.2$ than in the initial $l_\phi/l_f = 2.1$ cases. This gives rise to a greater rate of burning in the bi-modal distribution cases with initial values of $l_\phi/l_f = 5.5$ and 8.3 than in the initial $l_\phi/l_f = 2.1$ cases for initial $\phi' = 0.2$. The probability of finding highly reactive $1.0 \leq \phi \leq 1.10$ mixture is smaller for initial $l_\phi/l_f = 5.5$ cases than the initial $l_\phi/l_f = 2.1$ cases for bi-modal distribution with initial values of $\phi' = 0.4$ and 0.6. This gives rise to smaller mean value of burned gas mass $m_b(c \geq 0.9)$ for initial $l_\phi/l_f = 5.5$ cases than the initial $l_\phi/l_f = 2.1$ cases for bi-modal distribution. For cases with initial $l_\phi/l_f = 8.3$ the clouds of mixture inhomogeneities are relatively big (see Figure 1), and as a result, there is a high probability of obtaining a large region of almost homogeneous mixture in the vicinity of the center of the ignitor, which leads to a large variation of $m_b(c \geq 0.9)$ between different realizations. If the ignitor center is located in the vicinity of a large cloud of $1.0 \leq \phi \leq 1.1$, the slow burning rate in the pockets with $1.0 < \phi$ and $\phi > 1.1$ encountered during the expansion of hot gas kernel is mostly compensated by the high burning rate in the $1.0 \leq \phi \leq 1.1$ mixture and this leads to greater burned gas mass in the cases with initial $l_\phi/l_f = 8.3$ than in the cases with initial $l_\phi/l_f = 2.1$ for a given realization when the initial ϕ' is 0.4 and 0.6 for the bi-modal distribution. Furthermore, it has been demonstrated in Figure 7 that the burning rate assumes small values in the regions, which are associated with high values of N_ξ, and the probability of finding high values of N_ξ is greater in the cases with initial $l_\phi/l_f = 2.1$ than in the cases with initial $l_\phi/l_f = 8.3$. This also acts to increase the mean value of the burned gas mass $m_b(c \geq 0.9)$ in the bi-modal distribution cases with initial $l_\phi/l_f = 8.3$ in comparison to the corresponding initial $l_\phi/l_f = 2.1$ cases for initial $\phi' = 0.4$ and 0.6.

The summary of the effects of initial mixture distribution for different values of u', ϕ', and l_ϕ/l_f on the outcome of localized forced ignition in terms of self-sustained combustion is presented in Table 2. It can be seen from Table 2 that the initial bi-modal mixture distribution cases offer higher probability of obtaining self-sustained combustion than in the cases with initial Gaussian distribution for initial values of $\phi' = 0.2$ and $u'/S_{b(\phi=1)} = 6.0$. The temporal evolution of the mean and standard deviation of burned gas mass for all cases listed in Table 1 are re-plotted in Figure 10 to demonstrate the effects of different distribution of stratified mixtures in comparison to the homogeneous mixture (i.e., premixed) cases. It is evident from Figure 10 that both initial Gaussian and bi-modal distribution cases with small initial values of ϕ' and l_ϕ/l_f behave similar to homogeneous mixtures due to rapid mixing (i.e., sharp decay of ϕ'). Furthermore, Figure 10 shows that it is possible to achieve a higher value of $m_b(c \geq 0.9)$ than the corresponding homogeneous mixture case for a given realization for both Gaussian and bi-modal distribution cases but this propensity is higher in the initial bi-modal distribution cases than in the initial Gaussian distribution cases (see also Table 2). The variation of burned gas mass $m_b(c \geq 0.9)$ between different realizations increases with increasing l_ϕ/l_f and ϕ' for both bi-modal and Gaussian distributions of ϕ but the degree of variability is smaller for initial Gaussian distribution cases than in the initial bi-modal distribution cases. This behavior originates due to the higher probability of finding $\phi \approx 1.0$ ($\phi \neq 1.0$) in the initial Gaussian (bi-modal) distribution case than those with initial bi-modal (Gaussian) distribution cases.

The variability of burned gas mass is routinely obtained in the cylinder of IC engines due to cycle-to-cycle variations (Pera et al., 2013). The findings from Figures 8–10 reveal that the degree of variability of burning depends not only on ϕ' and l_ϕ but also on the nature of mixture distribution, which can be manipulated by careful design of the nozzle and fuel injection systems in IC engines. Moreover, in-cylinder turbulence together with injection characteristics can influence the values of u', ϕ', and l_ϕ, and thus the effective control of mixing characteristics in IC engine combustion chamber can potentially play a pivotal role in ensuring successful ignition and reducing the variability associated with the ignition event. Furthermore, the minimum ignition energy for ensuring self-sustained combustion subsequent to successful ignition in turbulent stratified mixtures is not only dependent on u', ϕ', and l_ϕ, but also on the nature of mixture distribution. This suggests that the success or failure of the ignition of stratified mixtures

Table 2. Summary of outcomes for the self-sustained combustion for all cases (✓ and × marks indicate the cases with successful self-sustained combustion following ignition and failed self-sustained combustion subsequent to forced ignition, respectively).

	$\phi' = 0.2$ [X]			$\phi' = 0.4$ [Y]			$\phi' = 0.6$ [Z]		
$\frac{L_{11}}{l_f} = 3.36$	$\frac{u'}{S_{b(\phi=1)}} = 0$ [T0]	$\frac{u'}{S_{b(\phi=1)}} = 4$ [T4]	$\frac{u'}{S_{b(\phi=1)}} = 6$ [T6]	$\frac{u'}{S_{b(\phi=1)}} = 0$ [T0]	$\frac{u'}{S_{b(\phi=1)}} = 4$ [T4]	$\frac{u'}{S_{b(\phi=1)}} = 6$ [T6]	$\frac{u'}{S_{b(\phi=1)}} = 0$ [T0]	$\frac{u'}{S_{b(\phi=1)}} = 4$ [T4]	$\frac{u'}{S_{b(\phi=1)}} = 6$ [T6]
$l_\phi/l_f = 2.1$	G:[✓][↓]	G: [✓][↑]	G: [×]	G: [✓][↓]	G: [✓][↑]	G: [×]	G: [✓][↓]	G: [✓][↑]	G: [×]
[D]	B:[✓][↓]	B: [✓][↓]	B: [✓][↑]	B: [✓][↓]	B: [✓][↓]	B: [×]	B: [✓][↓]	B: [✓][↓]	B: [×]
$l_\phi/l_f = 5.5$	G: [✓][↓]	G: [✓][↓]	G: [×]	G: [✓][↓]	G: [✓][↓]	G: [×]	G: [✓][↓]	G: [✓][↓]	G: [×]
[E]	B: [✓][↑]	B: [✓][↑]	B: [✓][↑]	B: [✓][↓]	B: [×]	B: [×]	B: [✓][↓]	B: [×]	B: [×]
$l_\phi/l_f = 8.3$	G: [✓][↓]	G: [✓][↓]	G: [×]	G: [✓][↓]	G: [✓][↓]	G: [×]	G: [✓][↓]	G: [✓][↓]	G: [×]
[F]	B: [✓][↓]	B: [✓][↓]	B: [✓][↑]	B: [✓][↓]	B: [✓][↓]	B: [✓][↑]	B: [✓][↓]	B: [✓][↓]	B: [×]

Note. Homogeneous cases: T0 [✓]; T4 [✓]; T6 [×]. [G]: Gaussian distribution; [B]: Bi-modal distribution.
[✓]: self-sustained combustion has been achieved; [×]: self-sustained combustion has not been achieved; [↑]: mean value of M_b is higher than homogeneous case; [↓]: mean value of M_b is lower than homogeneous case.

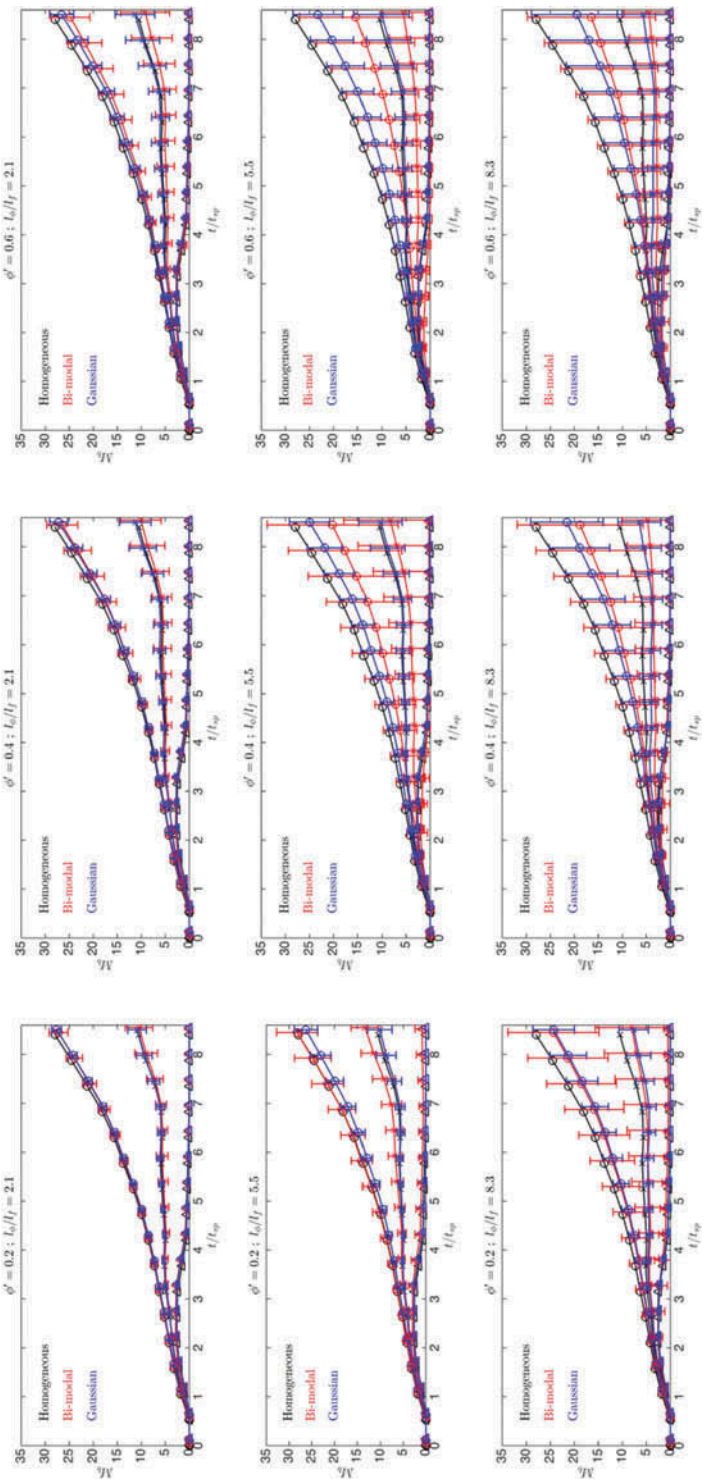

Figure 10. Temporal evolution of mean $M_b = \left[m_b(c \geq 0.9)\right] / \left[\{4/3\}\pi\rho_0 l_f^3\right]$ with standard deviation due to different realizations of initial conditions shown in the form of bars for all the cases with initial $u'/S_{b(\phi=1)} = 0.0$ [○], 4.0 [X], and 6.0 [Δ] for initial values of $\phi' = 0.2$ (1st column); 0.4 (2nd column); 0.6 (3rd column) and $l_\phi/l_f = 2.1$ (1st row); 5.5 (2nd row); and 8.3 (3rd row).

is a highly random event and that a small change in mixture distribution has the potential to alter the outcome. A limited number of simulations has also been carried out for globally fuel-lean (i.e., $\langle\phi\rangle = 0.8$) and the effects of u', ϕ', l_ϕ, and mixture distribution on localized forced ignition of $\langle\phi\rangle = 0.8$ mixtures have been found to be qualitatively similar to those in case of globally stoichiometric (i.e., $\langle\phi\rangle = 1.0$) mixtures but $\langle\phi\rangle = 0.8$ mixtures need a higher amount of energy than $\langle\phi\rangle = 1.0$ mixtures to successfully ignite and exhibit self-sustained combustion.

Conclusions

The effects of l_ϕ/l_f, ϕ', and $u'/S_{b(\phi=1)}$ on early stages of combustion following localized forced ignition of globally stoichiometric (i.e., $\langle\phi\rangle = 1.0$) stratified mixtures have been numerically investigated using 3D DNS simulations for both initial Gaussian and bi-modal distributions of equivalence ratio. The flame resulting from localized forced ignition shows a predominantly premixed mode of combustion although some pockets of the non-premixed mode of combustion have also been observed. The probability of finding non-premixed pockets is relatively greater in the case of initial bi-modal distribution than in the initial Gaussian distribution cases because the cases with initial Gaussian mixture distribution show greater probabilities of finding $\phi \approx \langle\phi\rangle = 1.0$ than the corresponding initial bi-modal distribution cases. The extent of non-premixed combustion decreases with decreasing (increasing) ϕ' and l_ϕ/l_f (u'). For a given value of l_ϕ/l_f, an increase in ϕ' leads to a reduction of burned gas mass for both Gaussian and bi-modal distributions, whereas the influence of l_ϕ/l_f on the extent of burning has been found to be non-monotonic and dependent on ϕ' for initial bi-modal mixture distributions, whereas the cases with initial Gaussian mixture distribution show an increase in burned gas mass with decreasing values of l_ϕ/l_f for all initial values of ϕ' considered here. The increase in heat transfer rate from hot gas kernel with increasing $u'/S_{b(\phi=1)}$ leads to a decrease in the extent of burning irrespective of the values of l_ϕ/l_f and ϕ' for both mixture distributions. However, some cases with initial bi-modal distribution show more resistance to flame extinction than the cases with initial Gaussian distribution for high values of $u'/S_{b(\phi=1)}$. The above findings demonstrate that the effects of l_ϕ/l_f, ϕ', and $u'/S_{b(\phi=1)}$ on the early stages of combustion following successful forced ignition of globally stoichiometric stratified mixtures are dependent on the nature of initial equivalence ratio distribution. Thus, it is not sufficient to characterize the minimum ignition energy of turbulent stratified mixtures in terms of l_ϕ/l_f, ϕ', and $u'/S_{b(\phi=1)}$, because it is possible to have successful self-sustained combustion for one type of mixture distribution but the same might not be true for a different type of mixture distribution with same set of values of l_ϕ/l_f, ϕ', and $u'/S_{b(\phi=1)}$. The qualitative nature of the present findings are not likely to change in the presence of detailed chemical kinetics but further analyses based on detailed chemistry and transport will be necessary for more comprehensive physical understanding and quantitative predictions.

Acknowledgments

The authors are thankful to N8/ARCHER for the computational support. The help provided by Mr. D. McKenna and Mr. Andrew Christie is also gratefully acknowledged.

Funding

The authors are grateful to EPSRC (EP/J003573/1 and EP/K025163/1) for the financial support.

References

Ahmed, S.F., and Mastorakos, E. 2006. Spark ignition of lifted turbulent jet flames. *Combust. Flame*, **146**, 215.

Anselmo-Filho, P., Hochgreb, S., Barlow, R., and Cant, R. 2009. Experiment measurements of geometric properties of turbulent stratified flames. *Proc. Combust. Inst.*, **32**, 1763.

Ballal, D.R., and Lefebvre, A. 1977a. Ignition and flame quenching in flowing gaseous mixtures. *Proc. R. Soc. London, Ser. A*, **357**, 163.

Ballal, D.R., and Lefebvre, A. 1977b. Spark ignition of turbulent flowing gases. AIAA Paper 77-185. Presented at the 15th Aerospace Sciences Meeting, Los Angeles, CA, January 24–26.

Ballal, D.R., and Lefebvre, A. 1980. A general model of spark ignition for gaseous and liquid fuel air mixtures. *Proc. Combust. Inst.*, **18**, 1737.

Balusamy, S., Cessou, A., and Lecordier, B. 2014. Laminar propagation of lean premixed flames ignited in stratified mixture. *Combust. Flame*, **161**, 427.

Batchelor, G.K., and Townsend, A.A. 1948. Decay of turbulence in final period. *Proc. R. Soc. London, Ser. A*, **194**, 527.

Bilger, R.W. 1988. The structure of turbulent non-premixed flames. *Proc. Combust. Inst.*, **23**, 475.

Chakraborty, N., Hesse, H., and Mastorakos, E. 2010. Effects on fuel Lewis number on localised forced ignition of turbulent mixing layers. Flow Turbul. Combust., 84(1), 125.

Chakraborty, N., and Mastorakos, E. 2008. Direct numerical simulation of localised forced ignition of turbulent mixing layers: The effects of mixture fraction and its gradient. *Flow Turbul. Combust.*, **80**(2), 155.

Chakraborty, N., Mastorakos, E., and Cant, R.S. 2007. Effects of turbulence on spark ignition in inhomogeneous mixtures: A direct numerical simulation (DNS) study. *Combust. Sci. Technol.*, **179**, 293.

Chen, J.H., Choudhary, A., de Supinski, B., DeVries, M., Hawkes, E.R., Klasky, S., Liao, W.K., Ma, K.L., Mellor-Crummey, J., Podhorski, N., Sankaran, R., Shende, S., and Yoo, C.S. 2009. Direct numerical simulations of turbulent combustion using S3D. *Comput. Sci. Discovery*, **2**, 015001.

Cruz, A.P.D., Dean, A.M., and Grenda, J.M. 2000. A numerical study of the laminar flame speed of stratified methane/air flames. *Proc. Combust. Inst.*, **28**, 1925.

Egolfopoulos, F.N., Cho, P., and Law, C.K. 1989. Laminar flame speeds of methane-air mixtures under reduced and elevated pressures. *Combust. Flame*, **76**, 375.

Espi, C.V., and Liñán, A. 2001. Fast, non-diffusive ignition of a gaseous reacting mixture subject to a point energy source. *Combust. Theor. Model.*, **5**, 485.

Espí, C.V., and Liñán, A. 2002. Thermal-diffusive ignition and flame initiation by a local energy source. *Combust. Theor. Model.*, **6**, 297.

Eswaran, V., and Pope, S.B. 1988. Direct numerical simulations of the turbulent mixing of a passive scalar. *Phys. Fluids*, **31**, 506.

Grune, J., Sempert, K., Kuznetsov, M., and Jordan, T. 2013. Experimental investigation of fast flame propagation in stratified hydrogen-air mixtures in semi-confirmed flat layers. *J. Loss Prev. Process Ind.*, **26**, 1442.

Haworth, D., Blint, R., Cuenot, B., and Poinsot, T. 2000. Numerical simulation of turbulent propane-air combustion with non-homogeneous reactants. *Combust. Flame*, **121**, 395.

Hélie, J., and Trouvé, A. 1998. Turbulent flame propagation in partially premixed combustion. *Proc. Combust. Inst.*, **27**, 891.

Huang, C.C., Shy, S.S., Liu, C.C., and Yan, Y.Y. 2007. A transition on minimum ignition energy for lean turbulent methane combustion in flamelets and distributed regimes. *Proc. Combust. Inst.*, **31**, 1401.

Im, H.G., Chen, J.H., and Law, C.K. 1998. Ignition of hydrogen-air mixing later in turbulent flows. *Proc. Combust. Inst.*, **28**, 1047.

Jiménez, C., Cuenot, B., Poinsot, T., and Haworth, D. 2002. Numerical simulation and modelling for lean stratified propane-air flames. *Combust. Flame*, **128**, 1.

Kang, T., and Kyritsis, D.C. 2005. Methane flame propagation in compositionally stratified media. *Combust. Sci. Technol.*, **177**, 2191.

Klein, M., Chakraborty, N., and Cant, R.S. 2008. Effects of turbulence on self-sustained combustion in premixed flame kernels: A direct numerical simulation (DNS) study. *Flow Turbul. Combust.*, **81**, 583.

Malkeson, S.P., and Chakraborty, N. 2010. Statistical analysis of displacement speed in turbulent stratified flames: A direct numerical simulation study. *Combust. Sci. Technol.*, **182**, 1841.

Mastorakos, E., Baritaud, T.A., and Poinsot, T.J. 1997. Numerical simulations of autoignition in turbulent mixing flows. *Combust. Flame*, **109**, 198.

Mulla, I.A., and Chakravarthy, S.R. 2014. Flame speed and tangential strain measurements in widely stratified partially premixed flames interacting with grid turbulence. *Combust. Flame*, **161**, 2406.

Neophytou, A., Mastorakos, E., and Cant, R.S. 2010. DNS of spark ignition and edge flame propagation in turbulent droplet-laden mixing layers. *Combust. Flame*, **157**, 1071.

Patel, D., and Chakraborty, N. 2014. Localised forced ignition of globally stoichiometric stratified mixtures: A numerical investigation. *Combust. Theor. Model.*, **18**(7), 627–651.

Pera, C., Chevillard, S., and Reveillon, J. 2013. Effect of residual burnt gas heterogeneity on early flame propagation and on cyclic variability in spark-ignited engines. *Combust. Flame*, **160**, 1020–1032.

Poinsot, T., Candel, S., and Trouvé, A. 1995. Applications of direct simulation to premixed turbulent combustion. *Prog. Energy Combust. Sci.*, **21**, 531.

Poinsot, T., and Lele, S.K. 1992. Boundary conditions for direct simulation of compressible viscous flows. *J. Comput. Phys.*, **101**, 104.

Renou, B., Samson, E., and Boukhalfa, A.M. 2004. An experimental study of freely-propagating turbulent propane-air flames in stratified inhomogeneous mixtures. *Combust. Sci. Technol.*, **176**, 1867.

Rogallo, R.S. 1981. Numerical experiments in homogeneous turbulence. NASA Technical Memorandum 81315, NASA Ames Research Center, California.

Samson, E. 2002. Etude experimentale de la propagation de flames en expansion dans un milieu a richesse stratifiee. PhD thesis. CNRS, Rouen, France.

Swaminathan, N., Grout, R., and Mastorakos, E. 2007. Direct simulation of forced ignition in stratified turbulent mixture. In: *Proceedings of the 3rd European Combustion Meeting*, Chania, Greece.

Sweeney, M.S., Hochgreb, S., Dunn, M.J., and Barlow, R.S. 2013. Multiply conditioned analyses of stratification in highly swirling methane/air flames. *Combust. Flame*, **160**, 322–334.

Tarrazo, E., Sanchez, A., Liñán, A., and Williams, F.A. 2006. A simple one-step chemistry model for partially premixed hydrocarbon combustion. *Combust. Flame*, **147**, 32.

Vedula, P., Yeung, P.K., and Fox, R.O. 2001. Dynamics of scalar dissipation in isotropic turbulence: A numerical and modelling study. *J. Fluid Mech.*, **433**, 29–60.

Wandel, A. 2013. Extinction predictor in turbulent sprays. Proc. Combust. Inst., 34, 1625.

Wandel, A. 2014. Influence on scalar dissipation on flame success in turbulent sprays with spark ignition. *Combust. Flame*, **161**, 2579.

Wandel, A., Chakraborty, N., and Mastorakos, E. 2009. Direct numerical simulations of turbulent flame expansion in fine sprays. Proc. Combust. Inst., 32(2), 2283.

Wray, A.A. 1990. Minimal storage time advancement schemes for spectral methods. NASA Report No. MS 202 A–1.

Yamashita, H., Shimada, M., and Takeno, T. 1996. A numerical study on flame stability at a transition point of jet diffusion flames. *Proc. Combust. Inst.*, **26**, 27.

Yu, R., and Bai, X.-S. 2013. Direct numerical simulation of lean hydrogen/air auto-ignition in a constant volume enclosure. *Combust. Flame*, **160**, 1706.

Zhou, J., Nishida, K., Yoshikazi, T., and Hiroyasu, H. 1998. Flame propagation characteristics in a heterogeneous concentration distribution of a fuel-air mixture. SAE Paper 982563.

Zhou, R., Balusamy, S., Sweeney, M., Barlow, R.S., and Hochgreb, S. 2013. Flow field measurements of a series of turbulent premixed and stratified methane/air flames. *Combust. Flame*, **160**, 2017.